

DOE Project

**Characterizing Ocean Acidification and Atmospheric Emission caused by Methane
Released from Gas Hydrate Systems along the US Atlantic Margin**

DOE Award No.: DE-FE0028980

Final Scientific/Technical Report

Period of Performance: 10/01/2016 to 09/30/2019

Principal Investigator:
John Kessler
University of Rochester



Co-Principal Investigator:
Carolyn Ruppel
US Geological Survey/Gas Hydrates Project
Woods Hole Coastal & Marine Science Center

June 22, 2020

DISCLAIMER:

This report was prepared as an account of work sponsored by an agency of the United States Government. Neither the United States Government nor any agency thereof, nor any of their employees, makes any warranty, express or implied, or assumes any legal liability or responsibility for the accuracy, completeness, or usefulness of any information, apparatus, product, or process disclosed, or represents that its use would not infringe privately owned rights. Reference herein to any specific commercial product, process, or service by trade name, trademark, manufacturer, or otherwise does not necessarily constitute or imply its endorsement, recommendation, or favoring by the United States Government or any agency thereof. The views and opinions of authors expressed herein do not necessarily state or reflect those of the United States Government or any agency thereof.

Abstract:

To assess the environmental impact of decomposing gas hydrates, this project characterized the atmospheric emission and ocean acidification associated with seafloor-released methane along the U.S. Atlantic Margin. This project leveraged the newly discovered seafloor seeps in this region, many of which are located near the landward limit of gas hydrate stability, to investigate the fate and environmental impact of methane once released from the seafloor.

Several research directions were pursued during these investigations. First, high-spatial resolution surface surveys were conducted to characterize the degree to which sea-to-air emission of methane is correlated with acoustically detected seafloor bubble emissions. Second, the natural isotopic signatures of both radiocarbon and $\delta^{13}\text{C}$ were measured throughout the water column to observe if seafloor-released methane was detected in surface waters or if it was replaced by a different source. Third, the extent of methane oxidation in the water column was constrained to assess the ability of this process to mitigate atmospheric methane emissions. Fourth, since aerobic methane oxidation ultimately converts methane to carbon dioxide, the extent of ocean acidification relating to this process was assessed.

Ultimately, this project was conducted in four stages. Stage one involved preparations for the research expedition along the U.S. Atlantic Margin. This involved calibrating, modifying, and validating equipment needed for sample and data collection in this unique environment. Stage two involved executing the at-sea science. This research was conducted from 25 August to 5 September 2017 on the R/V *Hugh R. Sharp*. This expedition left from Lewes, Delaware and investigated the continental slope from approximately this latitude down to Cape Hatteras, North Carolina. Third, any samples unanalyzed on the research vessel were returned to the laboratory and measured. Fourth, the data were interpreted, and publications and presentations were prepared.

Table of Contents

Abstract.....	3
List of Acronyms	5
Executive Summary.....	6
1. Sample and Data Collection.....	8
1.1 Survey Region.....	8
1.2 Acoustic Surveys	9
1.3 High-Resolution Surface Water Surveys of Dissolved CH ₄ Concentration	12
1.4 Discrete Water Column Samples	14
1.4.1. Dissolved CH ₄ Concentration	14
1.4.2. $\delta^{13}\text{C-CH}_4$	14
1.4.3. Natural Radiocarbon Content of CH ₄ Dissolved in Seawater ($\Delta^{14}\text{C-CH}_4$)	14
1.4.4. DIC Concentration.....	15
1.4.5. DIC Radiocarbon ($\Delta^{14}\text{C-DIC}$).....	15
1.4.6. pH.....	15
2. Chemical and Isotopic Signatures of Methane Emitted from Seafloor Seeps Along the US Atlantic Margin.....	16
2.1. Concentration Ratios.....	16
2.2. Isotopes	16
2.2.1. Stable carbon isotopes of methane ($\delta^{13}\text{C-CH}_4$).....	16
2.2.2. Natural Radiocarbon of Methane Dissolved in Seawater	18
2.3. Conclusions.....	18
3. Comparing Methane Emissions from the Seafloor with those from the Sea Surface.....	19
3.1. Spatial correlation of acoustically detected bubbles and sea surface methane concentrations.....	19
3.2. Seafloor-to-sea surface water column profiles of methane natural radiocarbon.....	20
4. Fate of Methane Dissolved in Seawater.....	22
4.1. Introduction.....	22
4.2. Mixing to dilute seep methane concentrations.....	22
4.3. Aerobic microbial oxidation as a means to remove seep methane from seawater.....	23
4.3.1. Theory.....	23
4.3.2. Results.....	25
5. Influence of oxidized methane on ocean acidification.....	29
5.1. Introduction.....	29
5.2. Results.....	29
6. Conclusions.....	32
7. References.....	33
8. Journal publications, databases, conference papers, and presentations	37
8.1. Publications.....	37
8.2. Manuscripts Currently in Revision Prior to Submission	38
8.3. Databases	38
8.4. Ph.D. Dissertations.....	38
8.5. Conference Presentations.....	39
8.6. Presentations	40

List of Acronyms

α	isotopic fractionation factor
δR_0	isotopic value of seep methane at the point of emission from the seafloor
δR	isotopic value of seep methane after some oxidation has occurred
^{14}C	natural radiocarbon content
$\delta^{13}\text{C}$	natural stable carbon isotope content
μg	microgram
AMS	accelerator mass spectrometry
AUV	Autonomous Underwater Vehicle
CH_4	Methane
CO_2	Carbon Dioxide
CRDS	Cavity Ringdown Spectrometer
CTD	Conductivity, Temperature, Depth
DIC	Dissolved Inorganic Carbon
DOC	Dissolved Organic Carbon
DOE	U.S. Department of Energy
DSV	Deep Submersible Vehicle
GC-FID	Gas Chromatograph with a Flame Ionization Detector
HRS1713	Cruise number for the expedition conducted here
Hz	hertz
IRMS	Isotope Ratio Mass Spectrometer
kHz	kilohertz
L	liters
LPM	liters per minute
mg	milligram
NETL	DOE's National Energy Technology Laboratory
NOAA	National Oceanographic and Atmospheric Administration
NSF	National Science Foundation
pMC	Percent Modern Carbon
POC	Particulate Organic Carbon
Riv	River
ROV	Remotely-operated vehicle
R/V	Research vessel
TXSY	Station Identifiers (Transect 'X', Station 'Y')
UC	University of California
UR	University of Rochester
USAM	US Atlantic margin
USGS	United States Geological Survey
UV-Vis	Ultraviolet-Visible
VES	Vacuum Gas Extraction System

Executive Summary:

Gas hydrate is a solid, ice-like structure which traps globally significant quantities of methane (CH₄) in ocean sediments and forms when the necessary low temperature, high pressure, and high CH₄ concentration conditions are met. The low temperature and high pressure conditions found deeper in ocean basins protect gas hydrates from destabilization during ocean warming, but the shallowest gas hydrates are susceptible to degradation as ocean waters warm (e.g., Berndt et al., 2014; Kvenvolden and Rogers, 2005; Ruppel, 2011; Ruppel & Kessler, 2017). Two potential environmental impacts of the release of CH₄ due to decomposing gas hydrates are (1) atmospheric warming, if this potent greenhouse gas travels through oceanic water column and enters the atmosphere, and (2) ocean acidification, if this CH₄ is aerobically oxidized in seawater to carbon dioxide (CO₂). Since both of these impacts occur after hydrates have decomposed and CH₄ has been emitted from the seafloor, and since the marine gas hydrates most susceptible to degradation are those at the shallowest water depths, we used newly discovered CH₄ seeps at or near the landward limit of gas hydrate stability as a testbed to investigate the fate and environmental impacts of CH₄ released from the seafloor. More specifically, we investigated CH₄ seeps along the upper continental margin of the U.S. Atlantic Margin between Delaware and Cape Hatteras, North Carolina.

Several key findings of this research aid in the characterization of the environmental impacts of seafloor released CH₄.

- First, the sea-to-air emission of oceanic CH₄ displayed a heterogeneous concentration distribution of dissolved CH₄ in surface waters throughout much of the U.S. Mid-Atlantic Margin. Numerous “hot spots” of emission were observed, but no spatial correlation was seen between these enhanced surface emissions and seafloor bubble emissions, even when ocean currents were accounted for in a preliminary way.
- Second, the radiocarbon content of CH₄ emitted from the seafloor at the landward limit of gas hydrate stability was shown to be fossil or devoid of measurable radiocarbon in this region. Since the half-life of radiocarbon is 5730 years and natural radiocarbon becomes undetectable by modern measurement techniques after approximately 10 half-lives, this suggests that the age of carbon in these CH₄ seeps is older than roughly 57,000 years. However, as the radiocarbon content of CH₄ dissolved in seawater was measured at greater altitude above the seafloor, the fossil signal measured above seafloor seeps was replaced by a more modern CH₄ source closer to the sea surface. These results indicate that the source of CH₄ released from the seafloor is not what is ultimately released to the atmosphere.
- Third, the natural stable carbon isotopes of CH₄ ($\delta^{13}\text{C-CH}_4$) were measured and demonstrated that the CH₄ was formed by biogenic pathways. This chemical analysis further revealed significant isotopic fractionation in numerous samples, indicating that the majority of seafloor-released CH₄ was aerobically oxidized in seawater, limiting atmospheric emission.

- Fourth, high precision pH measurements and the natural radiocarbon content of dissolved inorganic carbon (DIC) were made along this corridor of seafloor seep emissions. Dissolved CO₂ is one component of DIC, and we hypothesized that if fossil CH₄ was being oxidized to CO₂ in the water column, we should observe a decrease in the radiocarbon content of DIC in areas of active seafloor CH₄ emission. Our results did display a correlation between enhanced DIC concentration and decreased pH, and the radiocarbon age of this DIC did show a slight decrease in the regions of highest seafloor emission. This suggests that the oxidation of seafloor released CH₄ is contributing to ocean acidification in this region, even though the contribution is slight.

1. Sample and Data Collection

1.1. Survey Region

Water samples and data were collected along the U.S. Atlantic Margin (USAM) onboard the R/V *Hugh R. Sharp* from 24 August – 7 September 2017, cruise number HRS1713. Over 300 seafloor CH₄ seeps were recently discovered on this part of the margin, ranging in depth from 53 m to 1612 m (Skarke et al., 2014). Most relevant for this project, many of these seeps lie at or within a few hundred meters shallower than the landward limit of gas hydrate stability (~575 m water depth; Brothers et al., 2014; Skarke et al., 2014; Ruppel and Waite, 2020). Since the landward limit of gas hydrate stability is most susceptible to destabilization due to warming seawater and because the water column is shortest in this environment (Ruppel and Kessler, 2017), we view this as an ideal region to test some of the potential environmental impacts associated with decomposing gas hydrates. The environmental impacts investigated here occur after CH₄ is emitted from the sediment surface, and thus, we view the depth of these seafloor emissions as more relevant to these investigations than whether these specific seeps result from hydrate decomposition.

Surface water CH₄ concentration and acoustic surveys were conducted almost continuously throughout this expedition from Delaware to Cape Hatteras, North Carolina. In addition, vertical water column samples were collected from 25 stations on seven downslope sampling transects, which spanned a 230 km corridor of the upper continental slope between northern Virginia and Cape Hatteras (Figure 1). Locations for the sample collection are labeled as TXSY, where T represents the transect, S represents the station along the transect, and X and Y are transect and station numbers, respectively. At these stations, discrete samples were collected via a carousel of Niskin bottles to sample seawater throughout the water column. The samples were collected in vials and cuvettes and preserved when not measured immediately using established and published protocols (see Section 1.4 below). In addition, large volume (i.e. >10,000 L) samples of seawater were processed throughout the water column at these stations to collect dissolved CH₄ for natural radiocarbon analysis. These discrete samples were used to assess the transfer of CH₄ from the seafloor to the sea surface, the aerobic oxidation of CH₄ in the water column, and ocean acidification caused by CO₂ produced from the oxidation of CH₄.

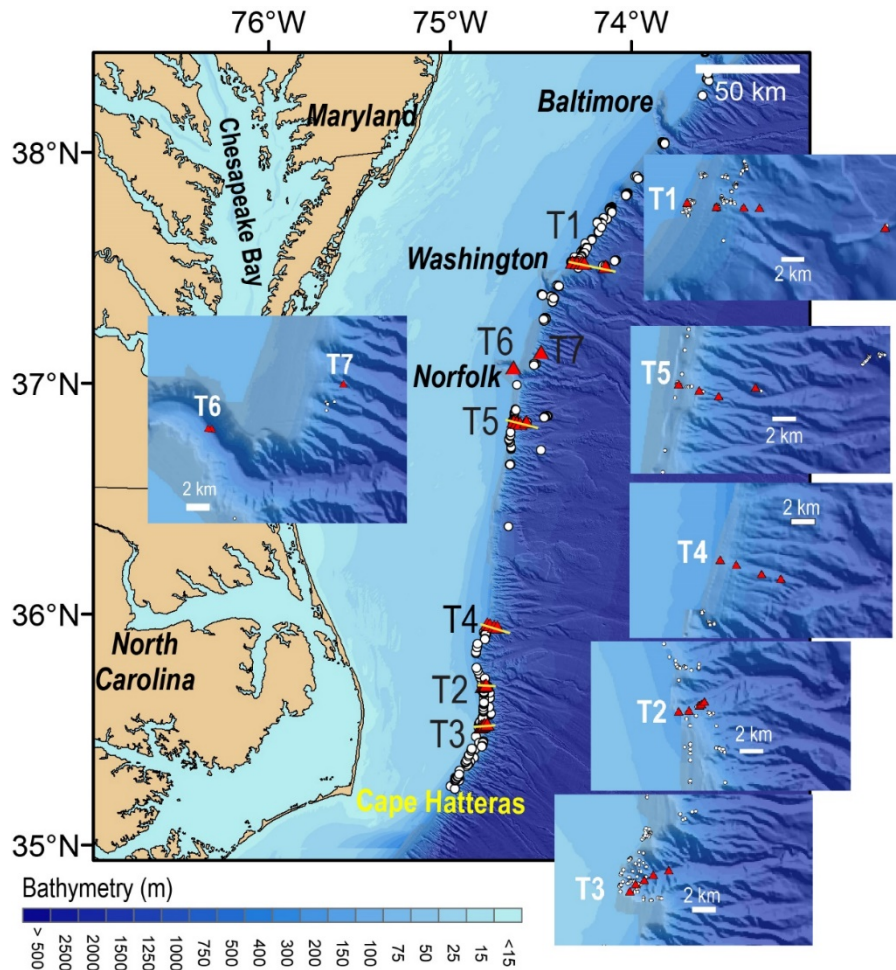


Figure 1. Map of sampling locations along the U.S. Atlantic Margin. In total, seven downslope transects were investigated, T1–T7. Red triangles show individual sampling stations that make up transects along the slope. White dots show gas seeps, either previously identified by Skarke et al. (2014) or detected during this cruise (Baldwin et al., 2020). Map and caption were originally published in Leonte et al. (2020).

1.2. Acoustic Surveys

In 2014, co-PI Ruppel collaborated with A. Skarke to release the first-ever compilation of CH₄ seep locations along the USAM north of Cape Hatteras (Supplement to Skarke et al., 2014). The seeps had been discovered based on the analysis of water column backscatter data collected by the EM302 (30 kHz) multibeam on NOAA’s *Okeanos Explorer* starting in ~2012. Prior to the Skarke et al., (2014) discovery of over 500 water column gas plumes along the USAM, only a few seeps had been known, notably at Blake Ridge and Baltimore Canyon.

Since 2015, the USGS, with support provided by DOE, has been using a portable fisheries sonar (EK60/80) equipped with a 38 kHz transducer mounted in a ship’s hull to image water column

CH₄ plumes during Atlantic margin research cruises. The principle of operation for the EK60/80 is similar to that for multibeam backscatter identification of plumes: The acoustic signal encounters a velocity difference when even small numbers of bubbles are present in the water column, and this manifests as a different strength for the returned acoustic signal.

The EK80 (broadband version of the EK60 transceiver) was used almost continuously during the HRS1713 cruise conducted for this project. This marked the first time that this technology had been applied to intensely survey for potential CH₄ seeps in the area near Cape Hatteras, the head of Keller Canyon, and in some other upper slope locations between Norfolk Canyon and Cape Hatteras. As one example of the results, the EK80 data were used to identify ~160 potential CH₄ plumes on the uppermost slope near the shelf break offshore Cape Hatteras, and many of these seeps had not previously been detected by Skarke et al., (2014). Reson 7160 multibeam water column imaging data (Baldwin et al., 2020) collected by the USGS in this area during the cruise provided further confirmation of some of the newly identified plumes.

Figure 2 shows a map from the area near Cape Hatteras with the tentative new plumes, along with the plumes reported by Skarke et al. (2014). As discussed elsewhere in this report, coincident sea-air CH₄ flux measurements, CTD casts, and other geochemical analyses permitted us to analyze the composition of gas bubbles, the impact of the plumes on the concentration of CH₄ in the water column in three dimensions, and the degree to which CH₄ emitted at the seafloor reached the sea-air interface. Seafloor explorations conducted with *DSV Alvin*, ROVs, and AUVs in the vicinity of identified water gas plumes at other locations along the USAM have almost always found indicators of past or contemporary CH₄ flux (e.g., benthic communities, authigenic carbonates, microbial mats) at the base of imaged water column CH₄ plumes, even if such studies have not always found the locus of gas emission or imaged bubbles emanating from the seafloor. Thus, we expect that eventual seafloor exploration of the newly identified potential gas plumes from cruise HRS1713 will eventually demonstrate that most of these plumes are also associated with seep indicators.

In 2018, A. Skarke, who had been using previously-unanalyzed *Okeanos Explorer* data to find more gas plumes on the USAM, and C. Ruppel, who was relying entirely on EK60/80 data collected for this project and others funded by the DOE-NETL CH₄ Hydrates R&D Program and NOAA Office of Ocean Exploration and Research, combined their new databases for a presentation to the Fall American Geophysical Union meeting (Skarke et al., 2018). This new database is the basis for a manuscript being prepared to update the USAM seeps inventory and for a USGS database that will be released to the public through Sciencebase.gov.

(Text in this paragraph is quoted with only minor modification from Leonte et al., 2020)
“The Simrad EK80 echosounder was also used to detect water column gas bubbles and to determine whether the CTD carousel was within a bubble plume during water sampling. This allowed us to determine when the water samples collected were directly influenced by gas bubble emissions, and thus constrain the chemical and isotopic signatures of CH₄ emitted from gas seeps. Figure 3 shows images generated by the echosounder as water samples were collected at T1S2 and T4S3, highlighting strong near-seafloor water column backscatter associated with gas bubbles for the first station and no such signal for the second one. It should be noted that the echosounder record collapses onto a flat display all detections within a conical ensonification

area beneath the EK80 transducer, and the ensonification cone is larger for greater water depths. In some cases, the CTD carousel appears to be within a backscatter cloud associated with a bubble plume, yet elevated CH₄ was not detected in the water samples. For example, the echosounder imaged strong near-seafloor backscatter at T5S2, but the water samples collected within the apparent bubble flare had CH₄ concentrations below 4 nM. This apparent contradiction could reflect the highly localized nature of fluctuations in CH₄ concentrations near the seafloor. Alternately, the enhanced backscatter imaged by the echosounder could represent bioscatters like krill instead of CH₄ bubbles.”

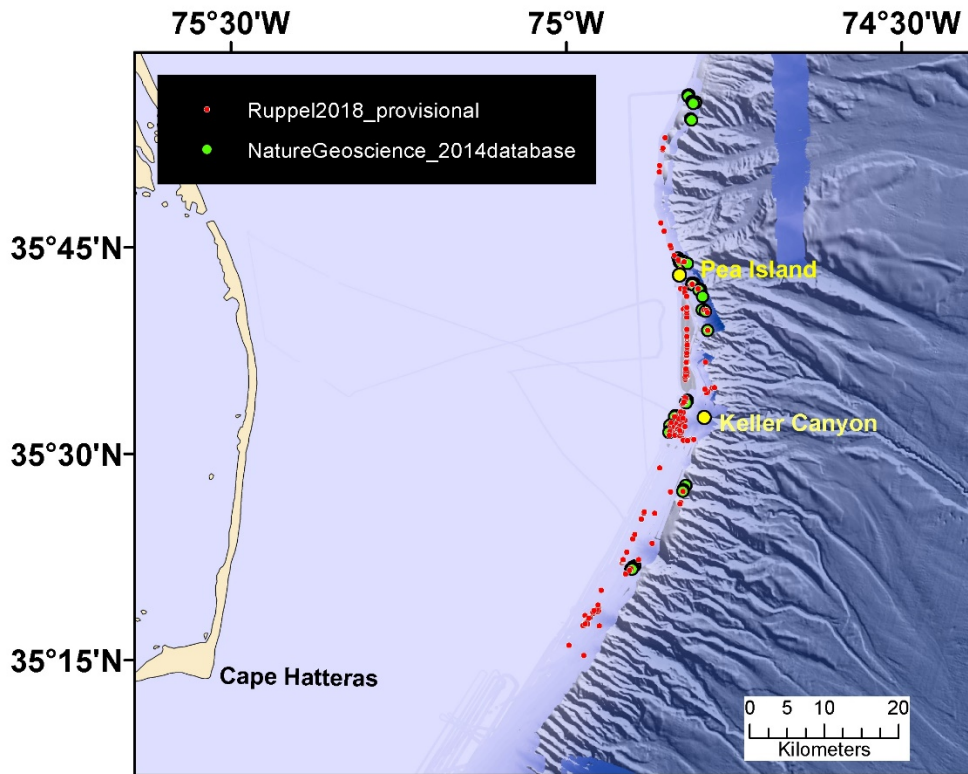


Figure 2. Preliminary identification of possible water column plumes (red) based on analysis of EK60/80 38 kHz data collected during the HRS1713 cruise. The green circles denote plumes identified in the database accompanying Skarke et al. (2014). Pea Island and Keller Canyon seeps (yellow) have been the site of seafloor explorations during various programs.

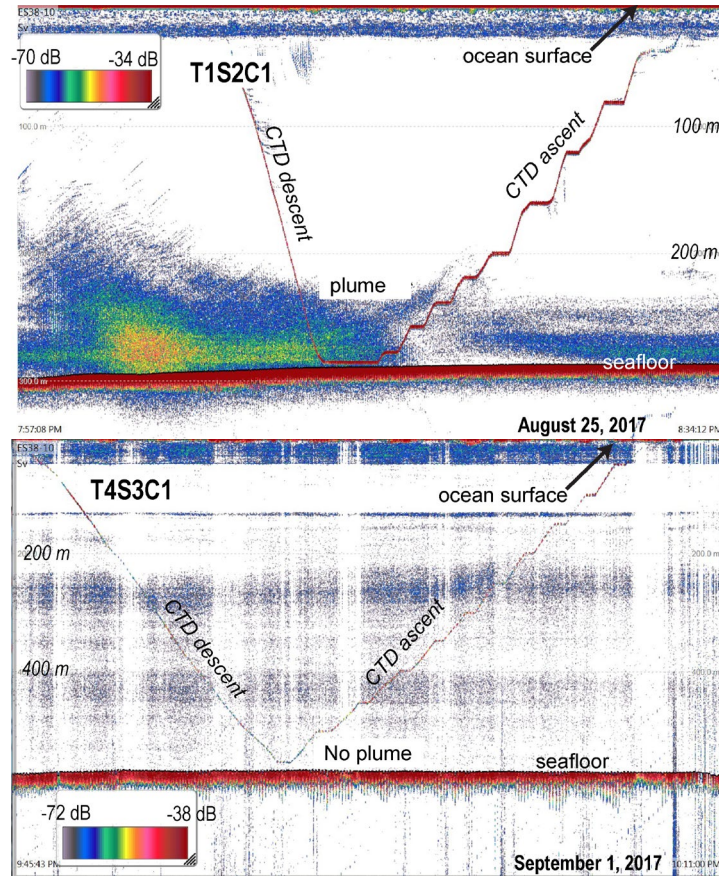


Figure 3. Acoustic echosounder images recorded at two sampling stations. The x-axis represents time, while the colored dots represent acoustic backscatter within the water column recorded by the echosounder. This may include suspended particles, gas bubbles, or the Niskin bottle carousel (red line). The top panel shows the image recorded at transect 1, station 2, CTD cast 1 where intense backscatter near the seafloor is indicative of gas bubbles, while the bottom panel was recorded at transect 4, station 3, CTD cast 1 where sparse backscatter suggests no bubbles were present. Figure and caption were originally published in Leonte et al. (2020).

1.3. High-Resolution Surface Water Surveys of Dissolved CH₄ Concentration

To more accurately resolve dissolved CH₄ concentrations in surface waters characterized by potentially strong spatial gradients, a vacuum extraction system (VES) for the ultra-fast, continuous, and automated analysis of dissolved CH₄ was developed with prior support from the National Science Foundation (OCE-1634871) (Figure 4). This system had been fully developed with systematic tests in the laboratory and across the U.S. Great Lakes and was further validated here before being used successfully along the continental slope of the USAM (Figure 6). The

VES method collects near-continuous data during surface water mapping and eliminates the disadvantage of slow equilibration times normally associated with seawater equilibrators by vacuum extracting the dissolved gases. Water is continuously pumped through a membrane contactor with a vacuum applied to the outside of the membrane; the dissolved gases travel through the membrane where they are continuously pumped into a Cavity-Ringdown Spectrometer (CRDS) for analysis. The degassed water and analyzed extracted gases are then continuously discarded overboard. With this experimental design, concentration changes in dissolved CH₄ concentration can be mapped with a resolution that is only limited by the time it takes to flush the system with the water and extracted gases, as well as the analysis time of the CRDS, which is in total a few seconds.

This new method contains three essential components: First, gases are vacuum extracted from a stream of water and are continuously pumped into a CRDS (Picarro G2201-i) for the measurement of CH₄ concentration and $\delta^{13}\text{C-CH}_4$ at analysis rates approaching 1 Hz. Second, the efficiency of the vacuum extraction for CH₄ is unknown, and it is further unknown how it may change with time and environmental conditions, so this system was continuously calibrated during our measurements along the US Atlantic Margin. Weiss-type equilibrators were used in parallel with the VES for the automated and continuous calibration of the vacuum gas extraction system (Figure 4). Routine calibration of the molar concentration also corrects for any sensor drift that may occur in the flow rate, temperature, and pressure measurements associated with this technique. The calibration is conducted by comparing the concentration determined with the Weiss-type equilibrators to that determined with the VES. While a Weiss equilibrator responds more slowly than the VES to changes in CH₄ concentration, the equilibrator concentration is independent of vacuum extraction efficiency. By continuously comparing values determined with the equilibrator to those determined with the VES, high and low equilibrator errors balance across a measurement period to establish a robust calibration. In addition to the continuous calibration with equilibrators, discrete seawater samples were also routinely collected for system calibration using a more conventional analysis technique with a gas chromatograph and flame ionization detector (GC-FID). Over the course of the research cruise along the USAM, we did not see

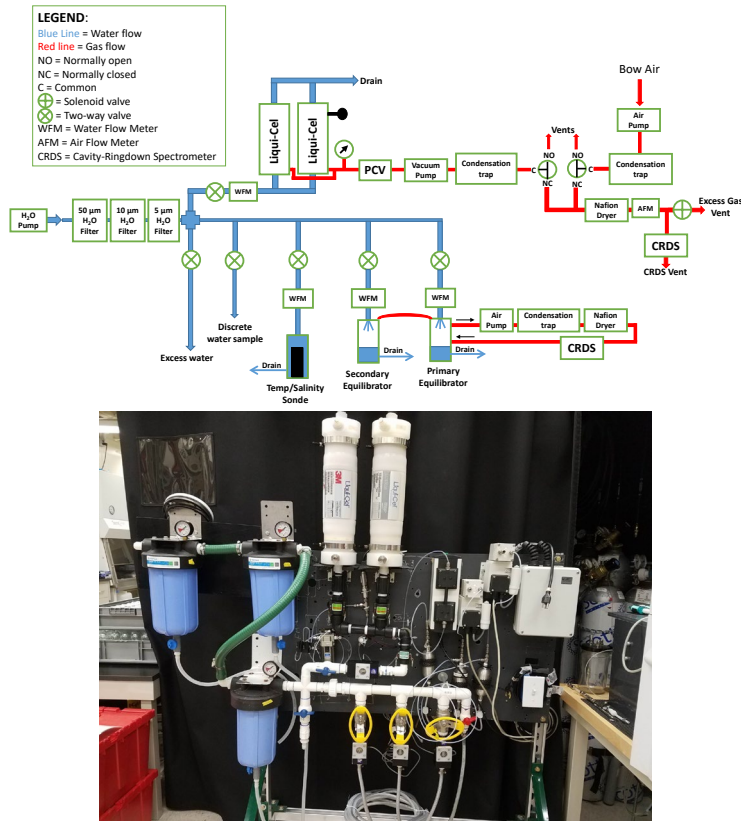


Figure 4. Schematic and photograph of the system used for the ultra-fast analysis of dissolved CH₄ concentration and $\delta^{13}\text{C-CH}_4$ in surface waters. The blue and red lines on the schematic indicate directions of water and gas flow, respectively.

changes in vacuum extraction efficiency and were able to establish robust calibrations. Third, electronics and software were developed to enable the automated analysis and user-defined control of the VES and equilibrator systems, while continuously logging numerous data parameters.

1.4. Discrete Water Column Samples

1.4.1. Dissolved CH₄ Concentration

During the collection of vertical water column samples, and periodically from the surface water system for routine calibration, discrete water samples were collected in serum vials for the analysis of dissolved CH₄ concentration. Published procedures were used to determine these dissolved concentrations, which are described in detail in Weinstein et al. (2016) and Leonte et al. (2017, 2020). In brief, serum vials were flushed and filled with seawater, capped, and a gaseous headspace of pure nitrogen was inserted while displacing an equal volume of water. The samples were then stored in an incubator allowing the dissolved gases to come to equilibrium with the gaseous headspace at a constant temperature. The headspace was then removed and its CH₄ concentration was determined with a GC-FID. The original concentration of CH₄ dissolved in seawater was then calculated using the concentration of CH₄ in the headspace, the volumes of the headspace gas and water, and the solubility of CH₄.

1.4.2. $\delta^{13}\text{C-CH}_4$

Water samples for $\delta^{13}\text{C-CH}_4$ analysis were measured in shore-based laboratories at the Woods Hole Isotope Laboratories. Water was collected in 500 mL glass serum bottles and sterilized through the addition of 100 μL of a supersaturated solution of mercuric chloride (HgCl_2). Compound specific ^{13}C analyses of CH₄ were performed using a Thermo Finnigan DeltaPlus XL IRMS coupled to an Agilent 6890 Gas Chromatograph (GC) via a Finnigan GCCIII combustion interface at the Woods Hole Isotope Laboratory. Detailed descriptions of the sampling and analysis procedures are found in Leonte et al. (2017, 2020).

1.4.3. Natural Radiocarbon Content of CH₄ Dissolved in Seawater ($\Delta^{14}\text{C-CH}_4$)

A newly developed technique was modified and used for the characterization of $\Delta^{14}\text{C-CH}_4$. This technique is a modification of a previous technique (Kessler and Reeburgh, 2005) that enhanced sensitivity to determine $\Delta^{14}\text{C-CH}_4$ in seawater with background concentrations of dissolved CH₄. Similar to the VES, this technique continuously vacuum extracts dissolved gases from seawater; however, because the amount of carbon needed for a natural radiocarbon measurement via accelerator mass spectrometry (AMS) is relatively large (ca. 200 $\mu\text{g C}$), the membranes and pumps are larger, enabling water pumping at rates of 200 LPM. Approximately 300 L of dissolved gases were extracted from seawater during the cruise, enabling the collection of mg quantities of CH₄ required for both AMS and isotope ratio mass spectrometry (IRMS) analyses. After the CH₄ in the collected samples was purified and prepared for analysis in the Kessler laboratory at the University of Rochester, they were analyzed at the Keck CCAMS facility at UC Irvine for radiocarbon analysis. A full description of these analytical procedures can be found here (Sparrow and Kessler, 2017). The modifications incorporated for this specific research where the ability to sample water up to depths of 500 m and the incorporation of an additional gas extraction membrane for increased sampling rates.

1.4.4. DIC Concentration

DIC samples were collected in 120 mL glass serum vials, preserved by adding 25 μ L of a saturated solution of mercuric chloride, and sealed with butyl rubber stoppers. The DIC samples were measured in the Kessler laboratory at the UR and not at sea due to the fragile nature of the glassware involved. DIC is determined by acidifying a known amount of seawater with cleaned phosphoric acid. By acidifying the sample, the carbonate equilibrium is shifted towards CO_2 . The resulting CO_2 is stripped out of the sample by an inert gas (N_2). The extracted CO_2 gas is subsequently quantified with a Picarro G1101-i Cavity-Ringdown Spectrometer (CRDS) for isotopic CO_2 . The $^{12}\text{CO}_2$ and $^{13}\text{CO}_2$ peaks from the CRDS are continuously recorded by the LabVIEW program, which also controls the DIC analyzer, and are integrated. Standards are run and compared against the samples for quantitative determination. More details of these procedures can be found in previous publications (Garcia-Tigreros and Kessler, 2018).

1.4.5. DIC Radiocarbon ($\Delta^{14}\text{C}$ -DIC)

Samples were collected in 60 mL I-Chem vials and analyzed at the Keck CCAMS facility following published procedures (Gao et al., 2014). Typical precisions following these procedures are $< 2 \%$, providing the most accurate and precise results of known analyses.

1.4.6. pH

High precision pH analyses were conducted at sea using established sampling and analysis protocols involving a UV-Vis spectrophotometer for pH analysis (Agilent, Cary-100; (Clayton and Byrne, 1993) and SOP6B in (Dickson, C. L. Sabine, J. R. Christian, 2007)). Additional details of these sample collection and analysis procedures can be found in Garcia-Tigreros and Kessler, (2018).

2. Chemical and Isotopic Signatures of Methane Emitted from Seafloor Seeps Along the US Atlantic Margin

The chemical and isotopic signatures of CH₄ emitted from several seafloor seeps were measured for two primary purposes. First, signatures near the seafloor were compared against those in the surface water to investigate the source of CH₄ emitted to the atmosphere. Second, the natural stable carbon isotopes of CH₄ were used to determine the extent that CH₄ was oxidized. However, these near-seafloor analyses have the additional benefit of suggesting how the seep CH₄ in this region was formed. We note that because these experiments were designed to collect samples to uncover and quantify the fate of CH₄ released from the seafloor, they were collected via Niskin bottle carousel or large volume pumping, as described above, and not via remotely operated vehicle (ROV) as would be necessary for a more systematic sampling of gas bubbles emitted throughout this corridor of seeps. Nonetheless, the co-located acquisition of both acoustic data (for bubble detection) and Niskin bottles or large pumping (for water sampling) enabled us to visualize the sampling equipment with relationship to the bubble plume to ensure that seep influenced water was likely being collected (Figure 3).

2.1. Concentration Ratios

The abundance of ethane, propane, and butane, in addition to CH₄, in seep gas has typically been used to discriminate between thermogenic versus microbial processes in CH₄ formation mechanisms. Biogenic formation processes are accepted as having minimal, if not undetectable, quantities of these higher order hydrocarbons. Several samples were collected during this expedition showing undetectable quantities of ethane, propane, and butane, suggesting the predominance of microbial formation mechanisms.

2.2. Isotopes

2.2.1. Stable Carbon Isotopes of Methane ($\delta^{13}\text{C-CH}_4$)

(Text in this section is quoted with only minor modification from Leonte et al., 2020)

“Stations at Transect 1 showed the greatest abundance of bubbles identified by the echosounder (Figures 1 and 3), and $\delta^{13}\text{C-CH}_4$ isotopic values measured on samples collected near this seafloor source ranged from -70.2‰ to -62.0‰. Among these, the sample with the lightest $\delta^{13}\text{C-CH}_4$ value, -70.2‰, and highest CH₄ concentration, 2.1 μM , was collected at Transect 1, Station 3. Due to these conditions, we consider the $\delta^{13}\text{C-CH}_4$ value of -70.2‰ to represent that emitted from gas seeps located near Transect 1. At transect 2, the highest CH₄ concentrations were all measured at a depth of 400 m for stations 3, 4, and 5. Although our echosounder readings did not detect a large abundance of water column bubbles at these stations, previous studies have identified a number of gas seeps near transect 2 (Figures 1 and 2), which could act as the dominant source of CH₄ at 400 m depth (Skarke et al., 2014). A Keeling plot was constructed to estimate the $\delta^{13}\text{C-CH}_4$ of CH₄ emitted from gas seeps near transect 2 (Figure 5). A Keeling plot can be used to estimate the isotopic signature of a given source term by calculating the linear least squares regression when plotting measurements of $\delta^{13}\text{C-CH}_4$ versus the inverse of CH₄ concentration (Keeling, 1958). The y-intercept represents the $\delta^{13}\text{C-CH}_4$ signature when the concentration of CH₄ from this source is infinite compared to the background. For our calculation, we used a geometric mean regression, rather than a least squares regression, to take

into account errors in both the x and y variables used in the Keeling plot (Pataki et al., 2003). This approach suggests the $\delta^{13}\text{C-CH}_4$ of CH_4 emitted from gas seeps near transect 2 was -53.4 ‰. Although certain measurements from transect 2 outside of the concentration plume at 400 m had lighter $\delta^{13}\text{C-CH}_4$ isotopic values than the samples used to construct the Keeling plot, they also had lower CH_4 concentrations, suggesting CH_4 was derived from a different source compared to the CH_4 plume identified at 400 m. The value of -53.4 ‰ implies that seeps in this region emit CH_4 with a heavier $\delta^{13}\text{C-CH}_4$ value than the seeps identified at transect 1. However, based on the Geometric Mean regression calculation, this value had an uncertainty of 7.2 ‰ due to the low sample size ($n = 3$) and variability of the data (Figure 5). Given the available data presented here, the value of $\delta^{13}\text{C-CH}_4$ emitted from seafloor seeps along the USAM was assumed to be within the range of -70.2 and -53.4 ‰.

“Based on the isotopic values of CH_4 emitted from gas seeps determined here (-70.2 to -53.4 ‰), this CH_4 is likely produced through microbial processes. In the subsurface shallower than 200 m depth, measurements of $\delta^{13}\text{C-CH}_4$ ranged between -65.4 ‰ and -42.1 ‰, suggesting that the CH_4 source in the subsurface is also of microbial origin. Although some samples collected shallower than 200 m depth have $\delta^{13}\text{C-CH}_4$ signatures heavier than the typical microbial production cutoff of -50 ‰, it is likely that when this CH_4 was produced, the $\delta^{13}\text{C-CH}_4$ values were within the microbial range and were later altered through microbial oxidation to a heavier value, as is evidenced by the concurrent shifts to lower dissolved concentrations (see Figure 11 in Section 4.3.2.). Thermogenic production, unlike microbial production, would also lead to the formation of longer chained hydrocarbons such as ethane, propane, and butane, which were below detection limits.”

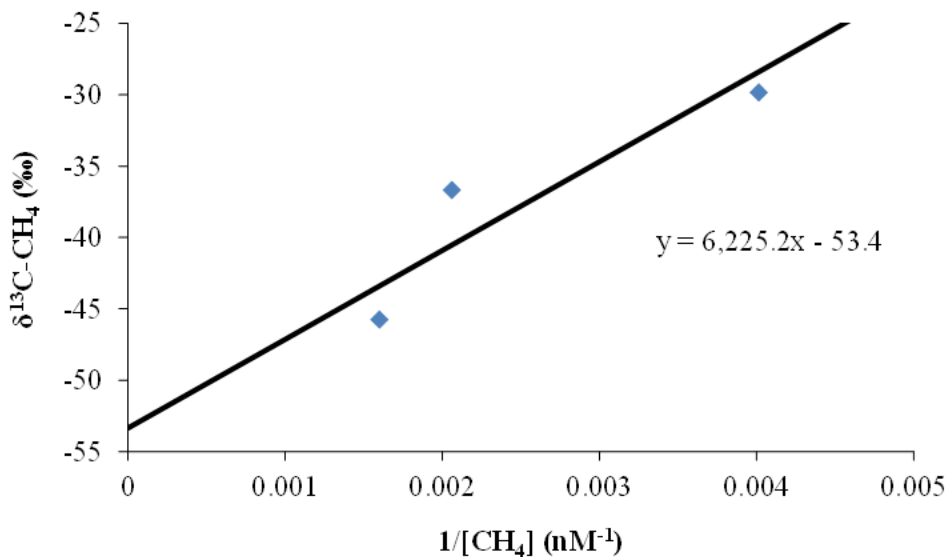


Figure 5. Keeling plot generated to determine the $\delta^{13}\text{C-CH}_4$ signature of CH_4 emitted from gas seeps. The Keeling plot was generated using CH_4 concentration and $\delta^{13}\text{C-CH}_4$ isotopic values measured at 400 m depth in transect 2. Using a geometric mean regression, the y-intercept, and thus the isotopic signature of CH_4 emitted from gas seeps at this location was -53.4 ± 7.2 ‰. Figure and caption were originally published in Leonte et al. (2020).

2.2.2. Natural Radiocarbon of Methane Dissolved in Seawater

Seawater was collected near emissions of CH₄ bubbles from the seafloor and processed for natural radiocarbon analysis using the techniques described above. In total, three bottom water samples were collected at stations T1S2, T3S3, and T7S1. All samples displayed radiocarbon values which were near fossil, with an average value of 3.2 pMC (see Figure 7 in Section 3.2). We interpret the values greater than 0 pMC to indicate that our large volume pumping system sampled some non-seep influenced water during the sample recovery process. However, the very low radiocarbon values imply that the vast majority of the sampling occurred in waters dominated by seep CH₄ inputs.

2.3. Conclusions

Taken together, the samples collected in this region indicate that CH₄ carbon released from these seafloor seeps is old and likely formed by biogenic mechanisms. We reiterate here that we did not conduct an exhaustive survey of seep CH₄ sources during this project. Rather, our investigations were designed to explore the fate of CH₄ once released from the seafloor near the landward stability limit of gas hydrates. Nonetheless, the near-seafloor samples we do have data for suggest the origin of CH₄ in this region is old biogenic CH₄.

3. Comparing Methane Emissions from the Seafloor with those from the Sea Surface

3.1. Spatial correlation of acoustically detected bubbles and sea surface methane concentrations

In our proposal for this project, we hypothesized that increases in dissolved CH₄ concentration in surface waters would be spatially located with acoustically detected seafloor seeps. To test this hypothesis, we mapped the dissolved concentration of CH₄ in surface waters with high spatial resolution while concurrently acoustically mapping seafloor bubble emissions. These mapping exercises were conducted nearly continuously when the ship was underway and not stationary collecting water column samples. Our focus was on seeps located along the upper continental margin near the calculated landward stability limit for gas hydrates.

From the data stream of dissolved CH₄ concentration collected as a function of time, we first investigated if enhancements or ‘hot spots’ in CH₄ concentration were observed. The locations of those CH₄ enhancements were then correlated with the locations of newly-detected and also previously known (Skarke et al., 2018) seafloor seeps. In order to objectively detect an enhancement in surface water dissolved CH₄ concentration, the first derivative was calculated on the time-course CH₄ concentration data. Values of zero for the first derivative were determined to be either peaks or valleys in CH₄ concentration. Next, the raw dissolved CH₄ concentration data was used to separate peaks from valleys. A peak was labeled if lower CH₄ concentration values were observed at the zero derivative points immediately before and after the point under investigation. Conversely, a valley was labeled if higher CH₄ concentration values were observed at zero derivative points immediately before and after the point under investigation. This algorithm identified 419 peaks of elevated CH₄ concentration during this expedition. This number is likely an underestimate as shoulders on peaks are ignored with this algorithm (Figure 6A).

The latitude and longitude of the 419 peaks were compared to those of the known and detected seafloor seeps (Figure 6B). While some sea surface CH₄ concentration peaks correlated with seafloor bubble emissions, many did not, and no statistically relevant correlation was identified. Even with the known currents in the area, the pattern of CH₄ concentration peaks relative to seafloor hotspots cannot be easily explained.

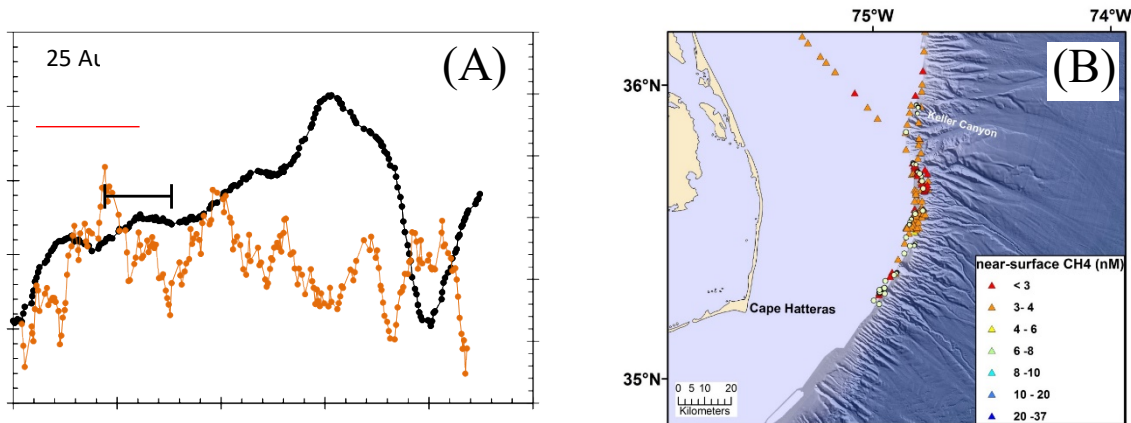


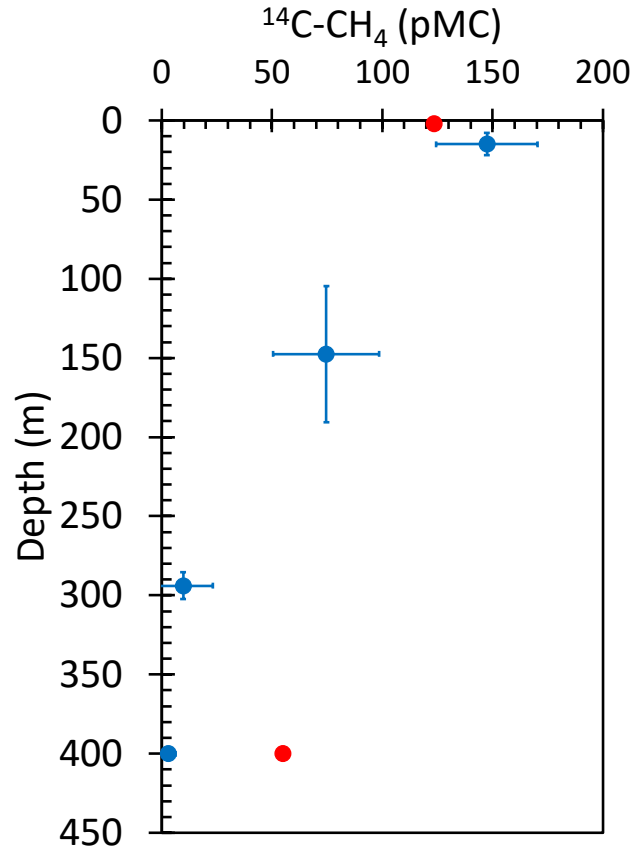
Figure 6. (A) Example data collected on 15 August 2017 to display the peak and valley data in surface water dissolved CH₄ concentration and $\delta^{13}\text{C}\text{-CH}_4$. (B) Locations of surface water ‘hot spots’ in dissolved CH₄ concentrations (triangles) and seafloor bubble emissions (circles) measured off the coast of North Carolina.

3.2. Seafloor-to-sea surface water column profiles of methane natural radiocarbon

To further investigate the transfer of CH₄ from the seafloor to the sea surface, we measured the natural radiocarbon content of CH₄ dissolved in the water column. These measurements were conducted at three stations with identified seep emissions (T1S2, T3S3, T7S1). In addition, one station with no seep emissions was analyzed (T6S1) and served as the background. Figure 7 displays the natural radiocarbon values for CH₄ dissolved in the seawater. For the stations measuring the water column above seafloor seeps, the bottom water impacted by seep emissions displayed near fossil radiocarbon values with an average of 3.2 ± 3.5 pMC. This result is similar to previously published results of CH₄ emitted from seafloor seeps or contained in gas hydrates at other locations (Kessler et al., 2008; Sparrow et al., 2018; and refers therein). However, as the altitude above the seafloor increased, the radiocarbon content increased and reached more modern values. We highlight that the radiocarbon units presented, percent Modern Carbon (pMC), are corrected for any isotopic fractionation (Stuiver and Polach, 1977), and thus the radiocarbon results display different sources of CH₄ carbon rather than the influence of isotopic fractionation, as might be expected for processes such as aerobic oxidation of CH₄. We further note that, while modern levels of atmospheric CO₂ are approximately 100 pMC, atmospheric CH₄ today has values closer to 135 pMC (Sparrow et al., 2018; Townsend-Small et al., 2012). This enrichment in atmospheric CH₄ is known to be due to the emission of the isotopomer ¹⁴CH₄ from nuclear power generation (Eisma et al., 1995; Graven et al., 2019; Lassey et al., 2007; Sparrow et al., 2018; Townsend-Small et al., 2012).

The transition from fossil CH₄ emitted from seeps and contained in bottom waters to more modern CH₄ closer to the sea surface indicates that seep CH₄ emitted here, at or near the landward limit of gas hydrate stability, was not being transferred to the surface waters and atmosphere. We extrapolate these results to conclude that CH₄ emissions from decomposing hydrates at the landward limit of gas hydrate stability is also unlikely to reach the ocean surface in mid-latitude regions.

Figure 7. Natural radiocarbon results for CH₄ dissolved in the water column along the USAM. Units are in percent Modern Carbon (pMC). The blue circles present the averages for samples collected above seafloor seeps at stations T1S2, T3S3, and T7S1. The error bars represent the natural spread in the data between stations rather than the analytical uncertainty. The red circles represent samples collected at a station without identified seafloor seeps (T6S1).



4. Fate of Methane Dissolved in Seawater

4.1. Introduction

Our surface and acoustic surveys, coupled with our measurements of CH₄ natural radiocarbon dissolved in the water column, showed that CH₄ emitted from seafloor seeps is not transferred to the sea surface in this region. However, the radiocarbon data alone do not uncover whether the fate of CH₄ in this region is dilution to more background concentrations or microbial oxidation in the oceanic water column. To assess the impact that mixing with background water dilutes the seep CH₄ concentration, we conducted a two end-member mixing model with the natural radiocarbon and dissolved CH₄ concentration data. And to assess the impact that microbial oxidation biochemically converts seep CH₄ to biomass and CO₂, we exploit the systematic isotopic fractionation of the stable carbon isotopes of CH₄ ($\delta^{13}\text{C-CH}_4$) during microbial oxidation to quantify the extent of this process.

4.2. Mixing to dilute seep methane concentrations

If the concentration of seep CH₄ dissolved in the water column is controlled primarily by dilution with background water, the measured concentration of CH₄ should be inversely proportional to the measured content of CH₄ radiocarbon (Equation 1).

$$^{14}\text{C} - \text{CH}_{4(m)} = \frac{(C_{seep} \times f_{seep} \times ^{14}\text{C-CH}_{4(seep)}) + (C_{bkg} \times f_{bkg} \times ^{14}\text{C-CH}_{4(bkg)})}{C_m} \quad (1)$$

Here, f_{seep} and f_{bkg} represent fractions originating from each endmember, seep and background water, respectively, where $f_{seep} + f_{bkg} = 1$. Also, C_m , $seep$, and bkg , and $^{14}\text{C-CH}_{4(m)}$, $(seep)$, and (bkg) represent CH₄ concentrations and radiocarbon isotopic values measured at each site, source, and background, respectively.

We assume the seep CH₄ endmember is represented by the bottom sample collected at station T1S2 ($C_{seep} = 458$ nM, $^{14}\text{C-CH}_{4(seep)} = 0.1$ pMC, see Section 3.2 above) due to the acoustic detection of seafloor seeps, high CH₄ concentration, and low radiocarbon value. We further assume that the background dissolved CH₄ endmember is represented by the near surface sample at T1S2 due to the absence of acoustically detected seep bubbles, CH₄ concentration near atmospheric equilibrium, and more modern radiocarbon value ($C_{bkg} = 4.4$ nM, $^{14}\text{C-CH}_{4(bkg)} = 131.3$ pMC). This endmember data was used with Equation 1 to model the CH₄ radiocarbon as a function of dissolved CH₄ concentration (Figure 8).

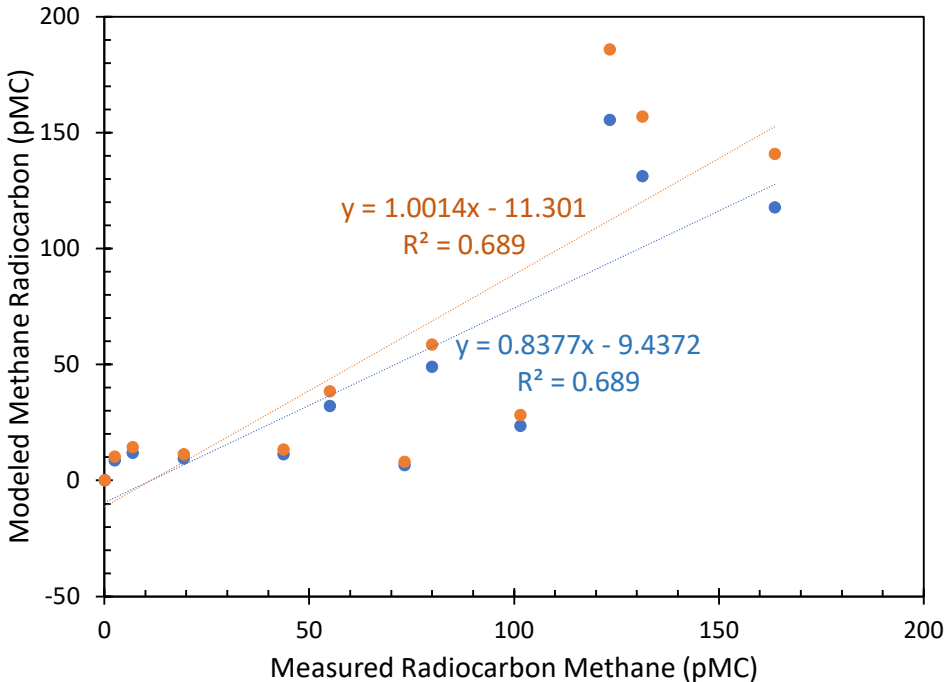


Figure 8. Modeling the dissolved CH₄ concentration and natural radiocarbon data with a two-endmember mixing model. Displayed is a correlation plot of the measured radiocarbon values versus the radiocarbon values modeled with a two-endmember mixing model. The blue points and linear correlation line incorporate the endmember data listed above. The orange points and linear correlation line incorporate the endmember data listed above, however, C_{bkg} is replaced with a value of 5.25 nM instead of 4.4 nM.

While there is some scatter, as indicated by the R^2 value of 0.689 in Figure 8, the measurements generally align with the mixing model. In addition, if the mixing model were a perfect representation of the processes controlling dissolved CH₄ distributions in this environment, the slope of the modeled versus measured results would be 1, not 0.838 as determined from the data collected, and the vertical axis intercept would be 0, not -9.44. However, we note that the modeled results are sensitive to the background endmember incorporated, and if the concentration of the background was 5.25 nM instead of 4.4 nM, the slope of this correlation plot would be 1 (Figure 8). Thus, it appears that mixing does play a significant role in decreasing the concentration of dissolved CH₄ in the water column, even if it does not fully describe all processes occurring.

4.3. Aerobic microbial oxidation as a means to remove seep methane from seawater

4.3.1. Theory

Once dissolved in seawater, microbially mediated aerobic methanotrophy can biochemically remove this CH₄, converting it to biomass and CO₂. This process can occur before, during, and after dilution decreases the concentration of seep CH₄ dissolved in seawater. Typically, aerobic

methanotrophy is assessed by measuring rates of this process that are specific to the location and time of sampling. These rates of methanotrophy are conventionally measured by adding minor amounts of isotopically labeled CH₄ to a sealed vial of seawater, incubating that seawater vial at in-situ temperatures, and quantifying the transfer of that isotopic tracer from reactant to product over the incubation time. However, in the present study, our interests are more in quantifying the total amount of CH₄ oxidized following seafloor emission to better understand how much CH₄ this process removes prior to atmospheric emission.

In order to constrain the fraction of seafloor-emitted CH₄ that has been aerobically oxidized in seawater, we rely on the systematic isotopic fractionation of the natural stable carbon isotopes of CH₄. The natural stable isotopes of CH₄ systematically change during the process of aerobic methanotrophy. This process often proceeds as a first-order chemical reaction (Eq. 2) and the rate constant for the ¹²CH₄ isotopologue is slightly larger than that for the ¹³CH₄ isotopologue. This leads to a preferential oxidation of ¹²CH₄ and an increase in the abundance to ¹³CH₄ relative to ¹²CH₄ in the residual CH₄. This process is typically characterized by the fractionation factor (α) which is defined as the ratio of the first-order rate constants for the light isotope over the heavy isotope. Thus, by measuring the change in the abundance ratio of ¹³CH₄ / ¹²CH₄ in the residual CH₄ following seafloor emission, the total extent of CH₄ oxidized can be determined.

$$\begin{aligned} \frac{d[^{12}\text{CH}_4]}{dt} &= -k_{12}[^{12}\text{CH}_4] \\ \frac{d[^{13}\text{CH}_4]}{dt} &= -k_{13}[^{13}\text{CH}_4] \\ \alpha &= \frac{k_{12}}{k_{13}} \end{aligned} \tag{2}$$

The theoretical details of this process are described in Leonte et al. (2017). In brief, after CH₄ is emitted from the seafloor and dissolved in a parcel of water, and thus available for oxidation, this chemical and isotopic process can be modeled as either a closed or open system. In a closed system, the reacting water parcel is viewed as a closed reacting ‘beaker’ and does not mix with neighboring water parcels. This closed parcel of water can be transported via advection, but it does not mix with water containing elevated concentrations of CH₄, thus following a Lagrangian approach. The open system allows complete mixing with neighboring water parcels as water advects along a trajectory, thus following an Eulerian approach. In both the closed and open systems, CH₄ continuously reacts following first-order kinetics, an assumption that was tested and determined to be true during a controlled incubation study of CH₄ oxidation (Chan et al. 2019). The box models, differential equations, and final derived equations used to determine the fraction oxidized (f), are found in Figure 9.

Model	Box model drawing	Differential Equations	Model equation
Rayleigh System		$\frac{d[H]}{dt} = -k_H[H]$ $\frac{d[L]}{dt} = -k_H[L]$	$f = 1 - \left(\frac{\delta R + 1000}{\delta R_0 + 1000} \right)^{\left(\frac{\alpha_c}{1 - \alpha_c} \right)}$
Open System		$\frac{d[H]}{dt} = \frac{r}{v}([H]_0 - [H]) - k_H[H]$ $\frac{d[L]}{dt} = \frac{r}{v}([L]_0 - [L]) - k_H[L]$	$f = \frac{\alpha_o}{1 - \alpha_o} \left(\frac{\delta R_0 + 1000}{\delta R + 1000} - 1 \right)$

Figure 9. Box model drawings, differential equations, and equation solutions for the closed (Rayleigh) and open system kinetic isotope models. The differential equations consider the change in concentration over time of heavy, $[H]$, and light, $[L]$, isotopes separately. Each model makes different assumptions regarding the processes that alter isotopic ratios. The closed system model assumes that only microbial oxidation influences isotopes. The open system assumes that both microbial oxidation and the mixing between CH_4 -rich water parcels will alter isotopic ratios. Mixing is assumed to be instantaneous and controlled by r , the flow rate of water into the box, and v , the volume of the box. For both models, the kinetic process of oxidation assumes a first-order reaction rate constant, k , which was later confirmed in Chan et al. (2019). Details in Leonte et al. (2017) show the algebraic steps necessary to derive the closed and open system model equations from the differential equations listed above. Figure and caption were originally published in Leonte et al. (2017).

In an accompanying study along the US Atlantic Margin in Hudson Canyon (Leonte et al., 2017), we determined that the closed system model more accurately described the results than the open system model and thus, we use that model to determine the fraction oxidized for the samples collected in 2017.

4.3.2. Results

In order to use the closed system model (Figure 9) to determine the fraction of CH_4 oxidized, both the fractionation factor (α) and the isotopic value at the point of emission into the water column (δR_0) must be known. The fractionation factor determined in Hudson Canyon, US Atlantic Margin, was applied to all samples collected in this study (Figure 1). The isotopic value at the point of emission into the water column was assumed to range from (-70.2‰ to -53.4‰) to encompass the values collected near the seafloor, as described in Section 2.2.1. above.

(Text in the following three paragraphs is quoted with only minor modification from Leonte et al., 2020.)

“Since we determined a range of values for δR_0 , the resulting calculations of the fraction oxidized (f) using the closed system model also produced a range of values. We calculated the maximum value of f when δR_0 was set to -70.2‰ and the minimum value of f when δR_0 was set to -53.4‰. For δR measurements lighter than -53.4‰, the minimum f value calculated was negative and thus set to 0. This situation implies that at a minimum, no oxidation had occurred at the time of sampling after the seep-derived CH₄ dissolved into the water column.

“Calculated f values show that CH₄ oxidation is an active process which has affected many of these samples to a large degree. Of the 75 samples collected from the deeper water column, below 200 m, and measured for CH₄ isotopic ratios, 7 had a minimum f value greater than 0.9 and 28, 47, and 54 samples had minimum f values greater than 0.7, 0.5 and 0.3, respectively. On the other hand, maximum f values suggest that 47 samples have over 90% of CH₄ removed through oxidation. The distribution of δR and f values was also correlated to the presence or absence of nearby gas seeps. Figure 10 shows a plot of the minimum CH₄ fraction oxidized, against $\delta^{13}\text{C-CH}_4$ isotopic values of samples collected from the deeper water column. Transects 1, 2, and 3, located close to gas seep clusters, showed an abundance of samples with f values as low as 0 due to significant CH₄ inputs from nearby seeps. However, samples from these transects also had a number of samples with f values close to 1 indicating a strong microbial oxidation signal despite the influence of gas seeps. For Transects 4, 5, 6, and 7, f values had a narrower range that was also shifted toward larger values of f due to a lack of active CH₄ inputs.

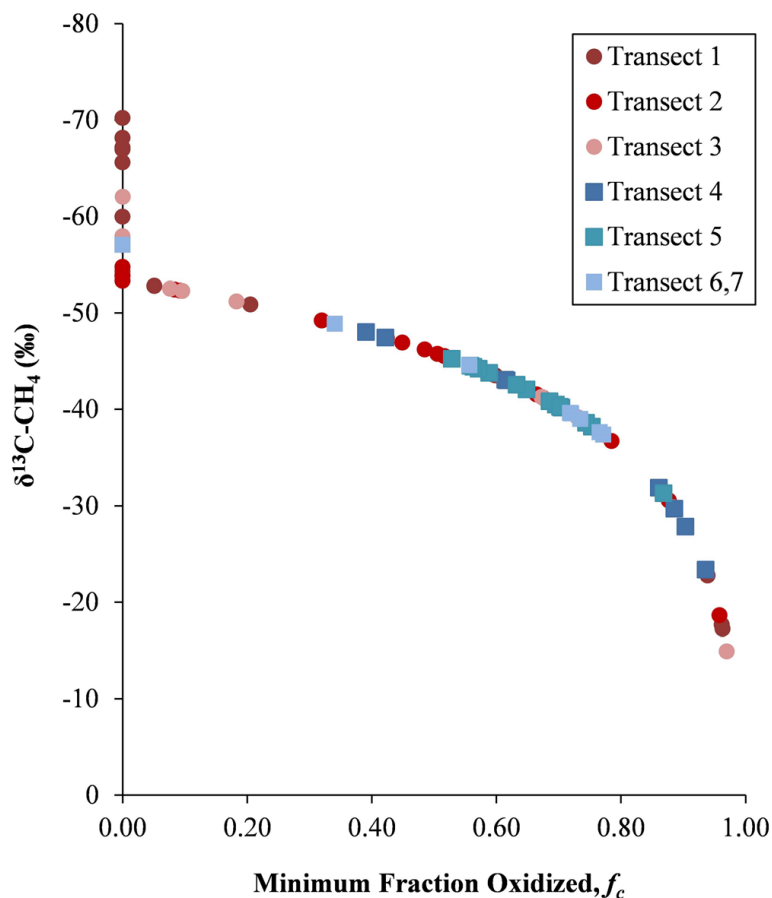


Figure 10. Plot of the minimum CH₄ fraction oxidized, f_c , against $\delta^{13}\text{C-CH}_4$ for samples collected along the USAM below 200 m. Circles show transects close to gas seeps (within 2.5 km) and likely receiving significant CH₄ inputs, while squares show transects farther than 2.5 km from gas seeps. Figure and caption were originally published in Leonte et al. (2020).

“Water column data collected within the subsurface also indicate a strong microbial oxidation sink. Figure 11 shows a plot of CH₄ concentration and $\delta^{13}\text{C-CH}_4$ measurements consistent with the expected trend produced through microbial oxidation: Lower CH₄ concentrations correlate with heavier $\delta^{13}\text{C-CH}_4$ values as oxidation progresses. As mentioned above, dividing the shallow water column samples based on the influence of nearby gas seeps results in different patterns regarding CH₄ concentration and $\delta^{13}\text{C-CH}_4$ measurements. Since $\delta^{13}\text{C-CH}_4$ values for samples affected by gas seeps within the subsurface (-65.4‰ to -54.8‰) are within the same range as CH₄ emitted from gas seeps within the deeper water column (-70.2‰ to -53.4‰), it is possible that this isotopic variation is entirely driven by the differences in CH₄ isotopes emitted from gas seeps. When calculating the fraction oxidized using a δR_0 value range of -70.2‰ to -53.4‰, the minimum f value for these samples was 0 while the maximum f value ranged from 0.37 to 0.91. For samples in the subsurface that were collected farther than 2.5 km from the nearest gas seep, the sample with the highest CH₄ concentration also had the lightest isotopic signature (-65.1‰), which we assume represents the isotopic signature for in situ methanogenesis (e.g. Repeta et al., 2016). Assuming $\delta R_0 = -65.1‰$, f was calculated based on the closed system equation (Figure 9). Values of f ranged from 0 to 0.88, implying a strong microbial oxidation sink. However, the closed system model assumes that no additional CH₄ is

added to a water parcel after the initial start of the oxidation reaction. Since in situ methanogenesis likely provides a semicontinuous flux of CH₄ to the water column, the quantity of CH₄ oxidized is likely underestimated using this model. Despite the CH₄ maximum observed between 100 and 200 m water depths, dissolved CH₄ concentrations quickly decreased to values near atmospheric equilibrium closer to the sea surface. This suggests that CH₄ oxidation is a thorough and near complete removal mechanism of dissolved CH₄ despite widespread gas seepage and aerobic methanogenesis along the USAM.”

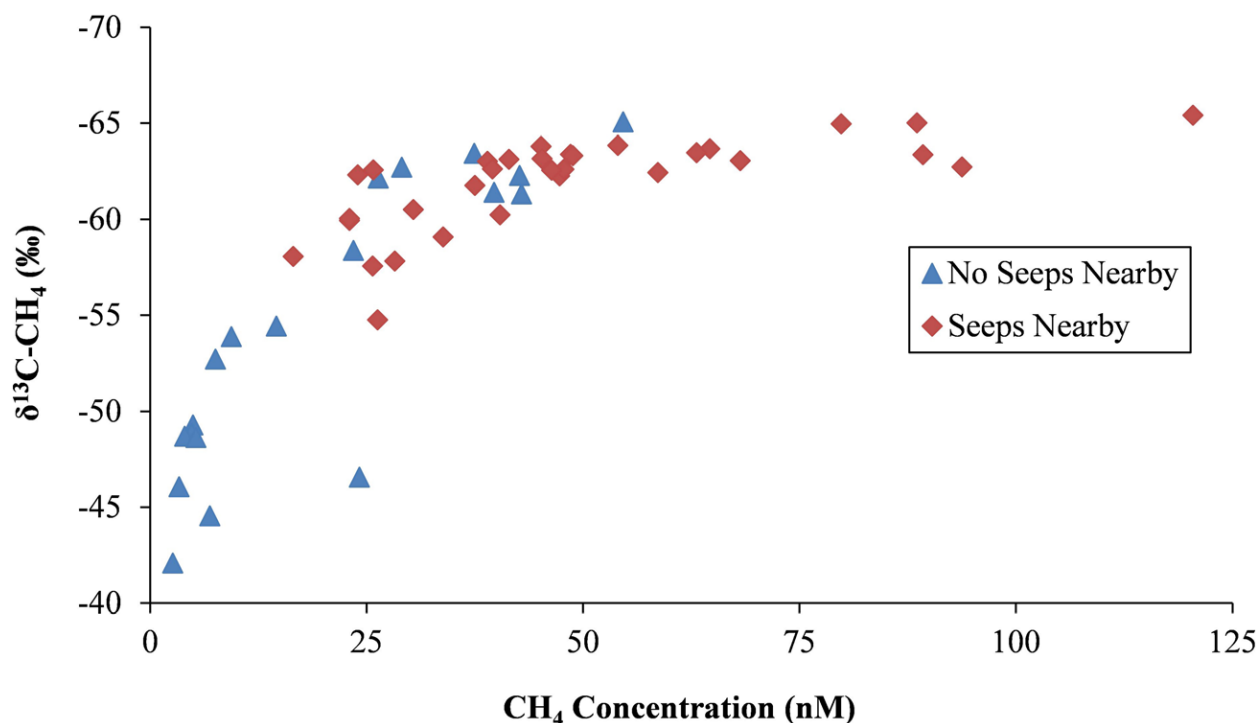
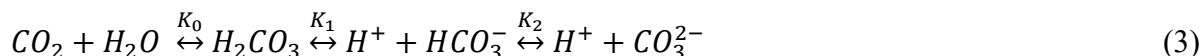


Figure 11. Plot of CH₄ concentration versus δ¹³C-CH₄ from samples collected in the subsurface or depths of 10 - 200 m along the USAM. Data are split up between stations without nearby gas seeps, blue triangles, and stations influenced by shallow water seafloor gas seeps, red diamonds. Stations designated to not be influenced by gas seeps were at least 2.5 km from the nearest identified gas seep using data collected here, Baldwin et al. (2020), and reported in Skarke et al. (2014). The higher CH₄ concentrations measured at stations closer than 2.5 km to identified gas seeps suggest that both aerobic production and gas seeps were supplying CH₄ to subsurface waters. Figure and caption were originally published in Leonte et al. (2020).

5. Influence of oxidized methane on ocean acidification

5.1. Introduction

The oxidation of CH₄ in an aerobic water column leads to the production of biomass intermediates and ultimately CO₂ (Chan et al., 2019). As described in Section 2, published radiocarbon values of CH₄ released from seafloor seeps have shown this CH₄ to be devoid of natural radiocarbon. This characteristic was confirmed for the seeps investigated in this study. Thus, any CO₂ produced from the oxidation of this seep CH₄ should also be devoid of natural radiocarbon. To explore the potential connection between the aerobic oxidation of seafloor-released CH₄ and ocean acidification, we acquired both high precision measurements of oceanic pH and natural radiocarbon of dissolved CO₂. However, we note that CO₂ once dissolved in seawater is not chemically inert; CO₂ inorganically reacts with water producing H₂CO₃, HCO₃⁻, and CO₃²⁻, chemically and isotopically in equilibrium with one another and with dissolved CO₂ according to their equilibrium partition constants (Eq. 3). The sum of dissolved CO₂, H₂CO₃, HCO₃⁻, and CO₃²⁻ is more generally defined as dissolved inorganic carbon (DIC).



Any background DIC to which fossil CO₂ is added from the oxidation of seep CH₄ would experience a decrease in the radiocarbon content. While measurement protocols for the concentration and natural radiocarbon content of DIC are established and where incorporated here (see Section 1), the main challenge is one of detection. Typical background concentrations of DIC in seawater are approximately 2000 μM whereas background CH₄ concentrations are closer to 2 nM, i.e. a factor of one million smaller. However, in CH₄ bubble plumes emanating from seafloor emissions, the concentration of dissolved CH₄ can reach the tens of micromolar range (Leonte et al., 2018). In this study, the concentrations reached as high as 2 μM (Leonte et al., 2020). Thus, if the seafloor emissions are significant and aerobic oxidation is efficient, a decrease in both pH and the natural radiocarbon of DIC is possible.

5.2. Results

Concurrent measurements of the dissolved concentration of DIC, ¹⁴C-DIC, and pH, along with CH₄ concentration and the oxidation rate of CH₄, were conducted along the main axis of Hudson Canyon, US Atlantic Margin during a cruise in 2014 (Garcia-Tigreros and Kessler, 2018; Leonte et al., 2017). While the current speed fluctuates and the current direction often reverses in this canyon, the longer-term direction of flow is down canyon (Rona et al., 2015). Here, both the radiocarbon of DIC and pH were observed to decrease down canyon (Figures 12 and 13).

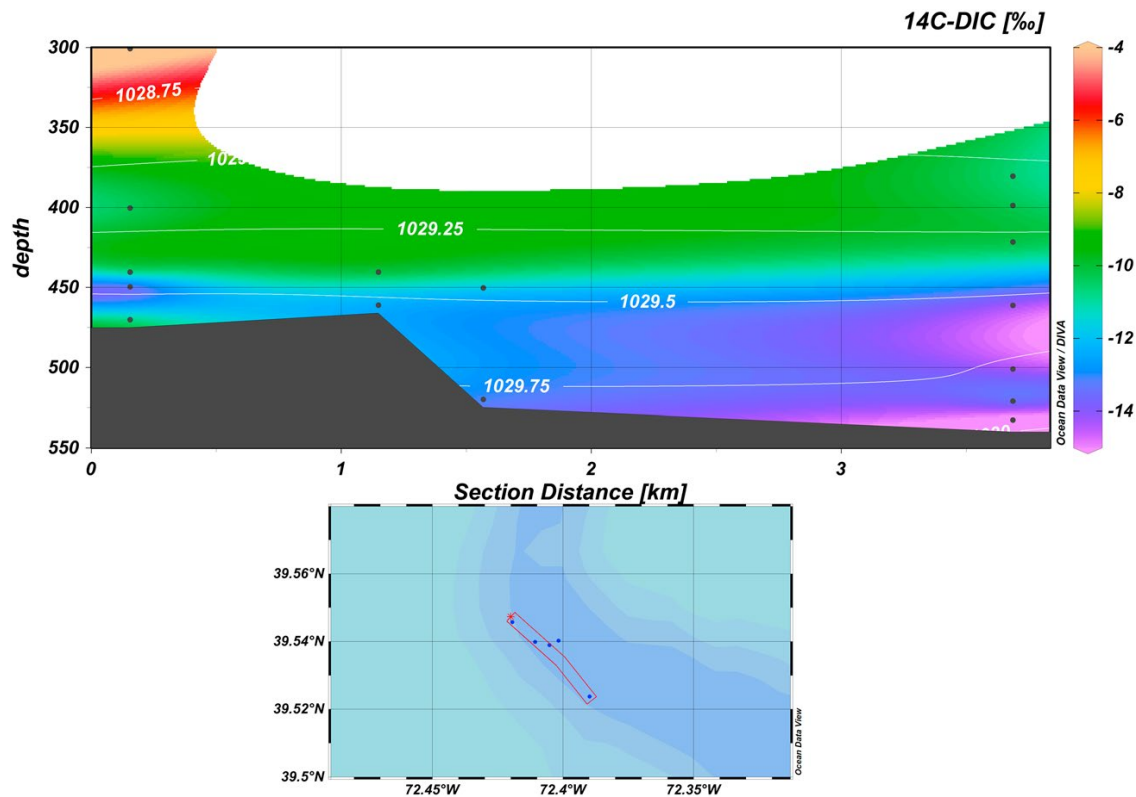
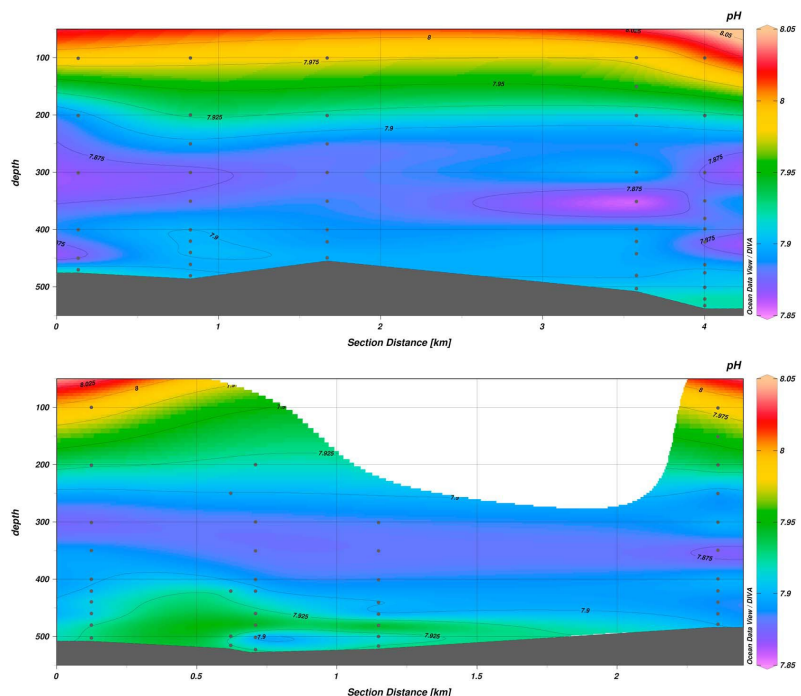


Figure 12. Radiocarbon transect from north to south of Hudson Canyon. The black dots represent discrete samples. The white contour lines represent isopycnals. Figure and caption were originally published in Garcia-Tigreros and Kessler, (2018).

Figure 13. Transects from north to south of the canyon for pH samples taken on west (top) and east (bottom) sides of the canyon. Figure and caption were originally published in Garcia-Tigreros and Kessler, (2018).



In this environment, all possible sources of this radiocarbon and pH reduction were investigated in a multicomponent mixing model, which included the respiration of marine dissolved organic carbon (DOC), marine particular organic carbon (POC), Hudson River dissolved organic carbon (riv), and seep CH₄ (CH₄), along with background DIC (b) (Figure 14). The solution of this radiocarbon mixing model (Eqs. 4 and 5) suggested that 0.3% of the DIC radiocarbon depletion in the region was from the oxidation of seep CH₄ (Garcia-Tigreros and Kessler, 2018).

$$^{14}\text{C}_s = (^{14}\text{C}_b \times f_b) + (^{14}\text{C}_{\text{DOC}} \times f_{\text{DOC}}) + (^{14}\text{C}_{\text{POC}} \times f_{\text{POC}}) + (^{14}\text{C}_{\text{CH}_4} \times f_{\text{CH}_4}) + (^{14}\text{C}_{\text{riv}} \times f_{\text{riv}}) \quad (4)$$

$$1 = f_b + f_{\text{DOC}} + f_{\text{POC}} + f_{\text{CH}_4} + f_{\text{riv}} \quad (5)$$

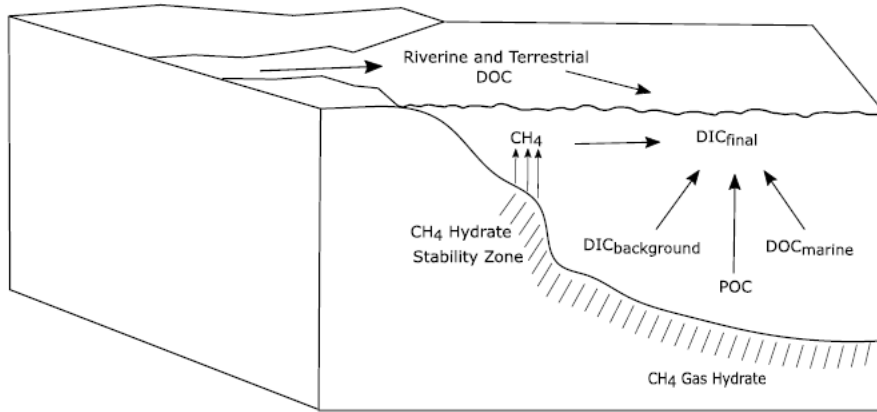


Figure 14. Potential ¹⁴C-DIC sources to Hudson canyon, USAM. Figure and caption were originally published in Garcia-Tigreros and Kessler, (2018).

A similar approach was taken when investigating the larger US Atlantic Margin based on the 2017 cruise conducted for this project. However, because the direction of ocean currents along the upper continental slope of this region is from the north to the south, we hypothesized that we would see a sequential addition of fossil CO₂ along this southward corridor, leading to the most substantial decreases in ¹⁴C-DIC and pH near Cape Hatteras (Figure 15).

However, our results did not reveal such a feature. No trend in ¹⁴C-DIC was observed from north to south; instead, the largest decreases in ¹⁴C-DIC were in the northern end of our study area. While our data do not show a sequential addition of fossil CO₂ along this ocean current trajectory, they did show that the largest additions of fossil CO₂ occurred in closest proximity to seafloor seeps. In the vertical water column, the largest decreases in ¹⁴C-DIC occurred at approximately 400 m depth, coincident with significant seafloor emissions of CH₄. These radiocarbon depletions were also accompanied by significant decreases in pH.

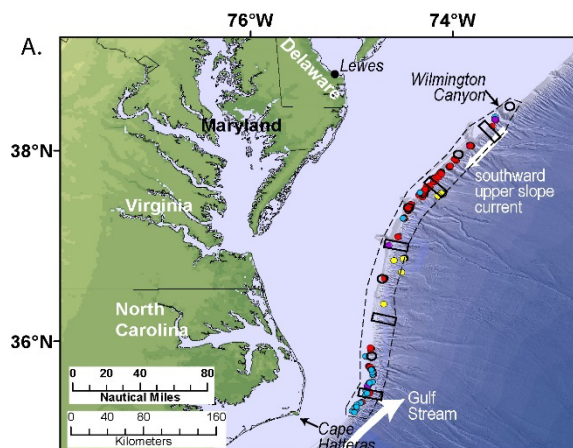


Figure 15. Occurrence of CH₄ seeps detected hydroacoustically along the northern USAM. The red, yellow, and purple circles indicate seeps in the original Skarke et al. (14) database. Blue circles are new seeps found by the USGS in April and September 2015 and aboard the R/V *Armstrong* verification cruise in March 2016. The dashed box encloses the study area. Black boxes and circles are nominal CTD transects and discrete CTDs, respectively, for the cruise conducted here. Current directions are indicated by the white arrows.

A radiocarbon isotopic mass balance was conducted (Eq. 6) to determine the fraction of the observed ¹⁴C-DIC that was ancient or fossil carbon.

$$^{14}\text{C}_{\text{obs}} = ^{14}\text{C}_{\text{Bkgd}} \cdot f_{\text{Bkgd}} + ^{14}\text{C}_{\text{Anc}} \cdot f_{\text{Anc}} \quad (6)$$

$$1 = f_{\text{Bkgd}} + f_{\text{Anc}}$$

This analysis showed that the highest fraction of ancient DIC occurred in the northernmost stations, closest to high abundances of seafloor seeps, resulting in a contribution of 1.5% ancient carbon. While this seems like a small percentage, we highlight that the annual increase in DIC concentration due to the oceanic uptake of atmospheric CO₂ in surface waters is roughly 0.1%. And even though seafloor CH₄ seeps are not as ubiquitous as atmospheric CO₂ uptake at the surface, we highlight seafloor seeps as a potentially significant source of CO₂ and ocean acidification in the mid-depths.

6. Conclusions

Overall, this research suggests that CH₄ emitted from oceanic gas hydrate systems, especially systems in mid-latitudes at the landward limit of hydrate stability, has minimal direct influence on the atmospheric CH₄ budget, in accordance with the analysis of Ruppel and Kessler (2017). However, dilution followed by aerobic CH₄ oxidation is significant at converting CH₄ to CO₂, which does appear to influence the dissolved inorganic carbon budget and pH of seawater if emissions are substantial and widespread.

7. References

- Baldwin, W.E., Moore, E.M., Worley, C.R., Nichols, A.R., and Ruppel, C.D., (2020). Marine Geophysical Data Collected To Support Methane Seep Research Along the U.S. Atlantic Continental Shelf Break and Upper Continental Slope Between the Baltimore and Keller Canyons During U.S. Geological Survey Field Activities 2017-001-FA and 2017-002-FA. Retrieved from U.S. Geological Survey data release. <https://doi.org/10.5066/P9Y1MSTN>
- Berndt, C., Feseker, T., Treude, T., Krastel, S., Liebetrau, V., Niemann, H., et al. (2014). Temporal constraints on hydrate-controlled methane seepage off Svalbard. *Science*, 343(6168), 284–287. <https://doi.org/10.1126/science.1246298>
- Brothers, L. L., Van Dover, C. L., German, C. R., Kaiser, C. L., Yoerger, D. R., Ruppel, C. D., et al. (2013). Evidence for extensive methane venting on the southeastern US Atlantic margin. *Geology*, 41(7), 807–810. <https://doi.org/10.1130/G34217.1>
- Chan, E.W., A.M. Shiller, D.J. Joung, E.C. Arrington, D.L. Valentine, M.C. Redmond, J.A. Breier, S.A. Socolofsky, and J.D. Kessler (2019). Investigations of Aerobic Methane Oxidation in Two Marine Seep Environments: Part 1-Chemical Kinetics. *Journal of Geophysical Research: Oceans*. <https://doi.org/10.1029/2019JC015594>
- Clayton, T. D., & Byrne, R. H. (1993). Spectrophotometric seawater pH measurements: total hydrogen ion concentration scale calibration of m-cresol purple and at-sea results. *Deep Sea Research Part I: Oceanographic Research Papers*, 40(10), 2115-2129, <https://doi.org/10.1017/CBO9781107415324.015>
- Dickson, A. G., Sabine, C. L., & Christian, J. R. (2007). Guide to best practices for ocean CO₂ measurements. In A. G. Dickson, C. L. Sabine, & J. R. Christian (Eds.). *N. P. M. S. Organization (Series Ed.), PICES Special Publication 3 (Vol. 3, pp. 191)*.
- Eisma, R., Vermeulen, A. T., and Van Der Borg, K. (1995). ¹⁴CH₄ emissions from nuclear power plants in Northwestern Europe. *Radiocarbon*, 37 (2), 475-483. https://doi.org/10.2458/azu_js_rc.37.1695
- Gao, P., Xu, X., Zhou, L., Pack, M. A., Griffin, S., Santos, G. M., et al. (2014). Rapid sample preparation of dissolved inorganic carbon in natural waters using a headspace-extraction approach for radiocarbon analysis by accelerator mass spectrometry. *Limnology and Oceanography: Methods*, 12(4), 174-190, <https://doi.org/10.4319/lom.2014.12.174>
- Garcia-Tigreros, F. and J. D. Kessler (2018). Limited acute influence of aerobic methane oxidation on ocean carbon dioxide and pH in Hudson canyon, northern U.S. Atlantic margin. *Journal of Geophysical Research: Biogeosciences*, 123(7), 2135-2144. <https://doi.org/10.1029/2018JG004384>

Graven, H., Hocking, T., and Zazzeri, G. (2019). Detection of fossil and biogenic methane at regional scales using atmospheric radiocarbon. *Earth's Future*, 7 (3), 283-299.

<https://doi.org/10.1029/2018EF001064>

Kessler, J.D. and W.S. Reeburgh (2005). Preparation of Natural Methane Samples for Stable Isotope and Radiocarbon Analysis. *Limnology and Oceanography: Methods*, 3, 408-418.

<https://doi.org/10.4319/lom.2005.3.408>

Kessler, J.D., W.S. Reeburgh, D.L. Valentine, F.S. Kinnaman, E.T. Peltzer, P.G. Brewer, J. Southon, and S.C. Tyler (2008). A survey of methane isotope abundance (^{14}C , ^{13}C , ^2H) from five nearshore marine basins that reveals unusual radiocarbon levels in subsurface waters.

Journal of Geophysical Research, 113(C12), C12021. <https://doi.org/10.1029/2008JC004822>

Kvenvolden, K. A., & Rogers, B. W. (2005). Gaia's breath—Global methane exhalations. *Marine and Petroleum Geology*, 22(4), 579–590. <https://doi.org/10.1016/j.marpetgeo.2004.08.004>

Lassey, K., Lowe, D., and Smith, A. (2007). The atmospheric cycling of radiomethane and the "fossil fraction" of the methane source. *Atmospheric Chemistry and Physics*, 7 (8), 2141-2149.

<https://doi.org/10.5194/acp-7-2141-2007>

Leonte, M., J. D. Kessler, M. Y. Kellermann, E. C. Arrington, D. L. Valentine, and S. P. Sylva (2017). Rapid rates of aerobic methane oxidation at the feather edge of gas hydrate stability in the waters of Hudson Canyon, US Atlantic Margin. *Geochimica et Cosmochimica Acta*, 204, 375-387.

<https://doi.org/10.1016/j.gca.2017.01.009>

Leonte, M., B. Wang, S. A. Socolofsky, S. Mau, J. A. Breier, and J. D. Kessler (2018). Using Carbon Isotope Fractionation to Constrain the Extent of Methane Dissolution Into the Water Column Surrounding a Natural Hydrocarbon Gas Seep in the Northern Gulf of Mexico.

Geochemistry, Geophysics, Geosystems. 19, 4459–4475. <https://doi.org/10.1029/2018GC007705>

Leonte, M., Ruppel, C. D., Ruiz-Angulo, A., and J. D. Kessler (2020). Surface methane concentrations along the Mid-Atlantic Bight driven by aerobic subsurface production rather than seafloor gas seeps. *Journal of Geophysical Research: Oceans*. 125, e2019JC015989.

<https://doi.org/10.1029/2019JC015989>

Pataki, D. E., Ehleringer, J. R., Flanagan, L. B., Yakir, D., Bowling, D. R., Still, C. J., et al. (2003). The application and interpretation of Keeling plots in terrestrial carbon cycle research.

Global Biogeochemical Cycles, 17(1), 1022. <https://doi.org/10.1029/2001GB001850>

Repeta, D. J., Ferrón, S., Sosa, O. A., Johnson, C. G., Repeta, L. D., Acker, M., et al. (2016). Marine methane paradox explained by bacterial degradation of dissolved organic matter. *Nature Geoscience*, 9(12), 884–887.

<https://doi.org/10.1038/ngeo2837>

Rona P., Guida V., Scranton M., Gong D., Macelloni L., Pierdomenico M., Diercks A. R., Asper V. and Haag S. (2015) Hudson submarine canyon head offshore New York and New Jersey: a physical and geochemical investigation. *Deep Sea Res. Part II* 121, 213–232.

<https://doi.org/10.1016/j.dsr2.2015.07.019>

Ruppel, C. D. (2011). Methane hydrates and contemporary climate change. *Nature Education Knowledge*, 2(12), 12.

Ruppel, C. D., & Kessler, J. D. (2017). The interaction of climate change and methane hydrates. *Reviews of Geophysics*, 55, 126–168. <https://doi.org/10.1002/2016RG000534>

Ruppel, C. D., & Waite, W. F. (2020). Grand Challenge: Timescales and Processes of Methane Hydrate Formation and Breakdown, with Application to Geologic Systems. *Journal of Geophysical Research: Solid Earth*, 125, e2018JB016459.

<https://doi.org/10.1029/2018JB016459>

Skarke, A. D., Ruppel, C. D., Kidiwela, M. W., Baldwin, W. E. & Danforth, W. W. (2018). Expanded U.S. Atlantic Margin Seep Inventory Yields Insight into Methane Dynamics, Fall Meeting, American Geophysical Union. OS33C-1913.

Skarke, A., Ruppel, C., Kodis, M., Brothers, D., & Lobecker, E. (2014). Widespread methane leakage from the sea floor on the northern US Atlantic margin. *Nature Geosci*, 7(9), 657-661.

Letter. <https://doi.org/10.1038/ngeo2232>

Sparrow, K. J. and J. D. Kessler (2017). Efficient collection and preparation of methane from low concentration waters for natural abundance radiocarbon analysis. *Limnology & Oceanography: Methods*, 15(7), 601-617. <https://doi.org/10.1002/lom3.10184>

Sparrow, K. J., J. D. Kessler, J. R. Southon, F. Garcia-Tiguerros, K. M. Schreiner, C. D. Ruppel, J. B. Miller, S. J. Lehman, and X. Xu (2018). Limited contribution of ancient methane to surface waters of the U.S. Beaufort Sea shelf. *Science Advances*, 4(1), eaao4842.

<https://doi.org/10.1126/sciadv.aao4842>

Stuiver, M., and H. A. Polach (1977). Discussion reporting of ^{14}C data. *Radiocarbon* 19, 355–363. <https://doi.org/10.1017/S0033822200003672>

Townsend-Small, A., Tyler, S. C., Pataki, D. E., Xu, X., and Christensen, L. E. (2012). Isotopic measurements of atmospheric methane in Los Angeles, California, USA: Influence of “fugitive” fossil fuel emissions. *Journal of Geophysical Research: Atmospheres*, 117 (D7).

<https://doi.org/10.1029/2011JD016826>

Weinstein, A., L. Navarrete, C. Ruppel, T. C. Weber, M. Leonte, M. Y. Kellermann, E. C. Arrington, D. L. Valentine, M. I. Scranton, and J. D. Kessler (2016). Determining the flux of

methane into Hudson Canyon at the edge of methane clathrate hydrate stability. *Geochem. Geophys. Geosyst.*, 17(10), 3882-3892. <https://doi.org/10.1002/2016GC006421>

8. Journal publications, databases, conference papers, and presentations

8.1. Publications

The following publications acknowledge this DOE project for support.

8) Leonte, M., Ruppel, C. D., Ruiz-Angulo, A., and J. D. Kessler (2020). Surface methane concentrations along the Mid-Atlantic Bight driven by aerobic subsurface production rather than seafloor gas seeps. *Journal of Geophysical Research: Oceans*. 125, e2019JC015989.

<https://doi.org/10.1029/2019JC015989> (peer-reviewed)

7) Leonte, M., B. Wang, S. A. Socolofsky, S. Mau, J. A. Breier, and J. D. Kessler (2018). Using Carbon Isotope Fractionation to Constrain the Extent of Methane Dissolution Into the Water Column Surrounding a Natural Hydrocarbon Gas Seep in the Northern Gulf of Mexico.

Geochemistry, Geophysics, Geosystems, 19. <https://doi.org/10.1029/2018GC007705> (peer-reviewed)

6) Kessler, J. K., C. D. Ruppel, D.-J. Joung, F. Garcia-Tigreros, and M. Leonte (2018).

Exploring Impacts of Widespread Seafloor Methane Seepage on Ocean Chemistry and Atmospheric Methane Emissions along the U.S. Mid-Atlantic Margin, [DOE Fire in the Ice hydrates newsletter](#), pp 4-6. (not peer-reviewed)

5) Sparrow, K. J. and J. D. Kessler (2018). Comment on “The origin of methane in the East Siberian Arctic Shelf unraveled with triple isotope analysis” by Sapart et al. (2017).

Biogeosciences, 15, 4777–4779. <https://doi.org/10.5194/bg-15-4777-2018> (peer-reviewed)

4) Garcia-Tigreros, F. and J. D. Kessler (2018), "Limited acute influence of aerobic methane oxidation on ocean carbon dioxide and pH in Hudson canyon, northern U.S. Atlantic margin."

Journal of Geophysical Research: Biogeosciences, 123(7), 2135-2144.

<https://doi.org/10.1029/2018JG004384> (peer-reviewed)

3) Sparrow, K. J., J. D. Kessler, J. R. Southon, F. Garcia-Tigreros, K. M. Schreiner, C. D.

Ruppel, J. B. Miller, S. J. Lehman, and X. Xu (2018), “Limited contribution of ancient methane to surface waters of the U.S. Beaufort Sea shelf.” *Science Advances*, 4(1), eaao4842.

<https://doi.org/10.1126/sciadv.aao4842> (peer-reviewed)

2) Sparrow, K. J. and J. D. Kessler (2017), “Efficient collection and preparation of methane from low concentration waters for natural radiocarbon analysis.” *L&O: Methods*, 15(7),601-617. <https://doi.org/10.1002/lom3.10184> (peer-reviewed)

1) Ruppel, C. D. and J. D. Kessler (2017), “The Interaction of Climate Change and Methane Hydrates.” *Reviews of Geophysics*, 55(1), 126-168. <https://doi.org/10.1002/2016RG000534> (peer-reviewed)

8.2. Manuscripts Currently in Revision Prior to Submission

- 1) Garcia-Tigreros, F., C. D. Ruppel, D.-J. Joung, M. Leonte, A. Ruiz Angulo, B. Young, J. D. Kessler (2020), “Estimating the impact of ancient methane on ocean pH and dissolved inorganic radiocarbon along the U.S. mid-Atlantic Bight.” *Journal of Geophysical Research-Biogeosciences*. *In Revision*.
- 2) Garcia-Tigreros, F., K. J. Sparrow, K. M. Schreiner, and J. D. Kessler, “Assessing acidification from the remineralization of dissolved organic carbon and methane in the coastal Beaufort Sea, Alaska.” *In Preparation*.
- 3) Joung, D.-J., M. Leonte, C. D. Ruppel, and J. D. Kessler (2019), “No emission of methane to the atmosphere from oceanic gas hydrates.” *In Preparation*.

8.3. Databases

CTD data measured on this cruise along with methane concentrations, isotopic ratios, and the fraction of methane oxidized can be accessed here (<https://accession.nodc.noaa.gov/0209090>).

Geophysical data used to identify gas seeps can be accessed here (<https://doi.org/10.5066/P9Y1MSTN>). This release also contains all of the other geophysical data collected during the cruise conducted for this study.

LADCP data can be accessed here (<https://accession.nodc.noaa.gov/0209236>).

pH, ^{14}C -DIC, and ^{14}C -CH₄ data is in preparation for archiving and will be submitted shortly.

8.4. Ph.D. Dissertations

- 1) Garcia-Tigreros Kodovska, F. (Defense Date: 17 April 2019). Assessing the Influence of Aerobic Methane Oxidation on Ocean Carbon Dioxide and pH, (Doctoral dissertation). Rochester, NY: University of Rochester.
- 2) Leonte, M. (Defense Date: 24 April 2019). Assessing Methane Dynamics In and Around Seafloor Gas Seep Environments Using Stable Isotopes, (Doctoral dissertation). Rochester, NY: University of Rochester.

8.5. Conference Presentations

Conference: American Geophysical Union Fall Meeting, Washington D.C., USA, December 10 – 14, 2018.

- 1) Authors: Fenix Garcia-Tigreros and John D. Kessler. Title: (Poster) Assessing the impact of aerobic methane oxidation on CO₂ chemistry in the U.S. mid-Atlantic Margin
- 2) Authors: Mihai Leonte, John D. Kessler, Carolyn D. Ruppel, and DongJoo Joung. Title: (Poster) Determination of Methane Sources and Sinks Using Stable Isotopes in Areas of Active Gas Seepage
- 3) Authors: Skarke, A. D., Ruppel, C. D., Kidiwela, M. W., Baldwin, W. E. & Danforth, W. W. Title: (Poster) Expanded U.S. Atlantic Margin Seep Inventory Yields Insight into Methane Dynamics.

Conference: Ocean Carbon and Biogeochemistry (OCB) Workshop on Oceanic Methane and Nitrous Oxide, UCLA Lake Arrowhead Conference Center, USA, October 28 – 31, 2018.

- 1) Author: John D. Kessler. Title (Invited Talk) Methane in the coastal shelf environment
- 2) Author: DongJoo Joung. Title (Poster) Radiocarbon measurements of methane dissolved in seawater near the upper edge of methane hydrate stability
- 3) Author: Mihai Leonte. Title (Poster) Determination of methane sources and sinks using stable isotopes in areas of active gas seepage
- 4) Author: Katy Sparrow. Title (Poster) Limited contribution of ancient methane to surface waters of the U.S. Beaufort Sea shelf

Conference: Gordon Research Conference on Natural Gas Hydrate Systems, Galveston, TX USA, February 25 - March 2, 2018.

- 1) Author: John Kessler. Title: (Invited Talk) High Resolution Measurements of the Sea-to-Air Flux of Methane Released from Hydrates
- 2) Author: Carolyn Ruppel. Title: (Invited Talk) Interaction of Deepwater and Permafrost-Associated Gas Hydrates with Climate Since the Last Glacial Maximum
- 3) Author: Mihai Leonte. Title: (Poster) Determination of Methane Sources and Sinks Using Stable Isotopes in Areas of Active Gas Seepage
- 4) Author: DongJoo Joung. Title: (Poster) Radiocarbon Measurements of Methane Dissolved in Seawater Near the Upper Edge of Methane Hydrate Stability

8.6. Presentations

1) Departmental Seminar (John Kessler)
University of North Carolina Chapel Hill
Department of Marine Sciences
October 11, 2017

Title: The Briny Blue Bubble Bender: Investigations of the chemical and isotopic kinetics of aerobic methane oxidation

2) Departmental Seminar (Carolyn Ruppel)
University of New Hampshire
Center for Coastal and Ocean Mapping
February 16, 2018

Title: An Update on the U.S. Northern Atlantic Margin Seep Province: Five Years Later